08

# Resistance change of thin films $Bi_2Se_3$ and heterostructures $Bi_2Se_3$ on graphene under tensile deformation

© N.A. Nebogatikova,[1] I.V. Antonova,[1,2] R.A. Soots,[1] K.A. Kokh,[3] E.S. Klimova,[3] V.A. Volodin[1,4]

[1] Rzhanov Institute of Semiconductor Physics, Siberian Branch, Russian Academy of Sciences,
630090 Novosibirsk, Russia
[2] Novosibirsk State Technical University,
630087 Novosibirsk, Russia
[3] Sobolev Institute of Geology and Mineralogy of the Siberian Branch of the RAS 630058 Novosibirsk, Russia
[4] Novosibirsk State University,
630090 Novosibirsk, Russia
e-mail: nadonebo@gmail.com, nadonebo@isp.nsc.ru

*Received November 13, 2023*
*Revised December 8, 2023*
*Accepted December 18, 2023*

The creation of vertical $Bi_2Se_3$ heterostructures based on graphene, obtained by physical vapor deposition, leads not only to a more advanced structure and conductivity of the $Bi_2Se_3$ layer, but also to improved mechanical properties. Films $Bi_2Se_3$ with a thickness of 20–40 nm based on CVD graphene slightly changed their resistance under tensile deformations created during bending of the structures. It was found that the resistance increases by only 20–30% when stretched to 3.3%. When $Bi_2Se_3$ is grown on a layer of printed graphene, a film $Bi_2Se_3$ is formed that is inhomogeneous in area and thickness, cracking at strains greater than 1.5%.

**Keywords:** vertical heterostructures, $Bi_2Se_3$ on graphene, tensile deformations, change in resistance.

DOI: 10.21883/0000000000

## Introduction

The development of technologies for the synthesis or layer-by-layer growth of vertical heterostructures from various 2*D*-materials is one of the main directions in the development of modern nanoelectronics [1,2]. Currently, graphene is widely used as a substrate for growing 2*D*-materials or quantum dots. Graphene, as a rule, increases the growth rate, improves the structure of the grown materials, or significantly affects the properties of the grown layer [3–6]. Currently, for heterostructures and for a topological insulator (in particular, $Bi_2Se_3$)/graphene are considered as a way to combine the spin-dependent properties of a topological insulator with high electron mobility in graphene [5]. It has been demonstrated that graphene provides a high-quality interface with thick films $Bi_2Se_3$ and high charge carrier mobility on surface topological states at low temperature [6–8]. In addition to spintronics, bilayer thin films have great potential for use in vertical heterostructures of 2*D*-materials as a channel with high conductivity.

Layers $Bi_2Se_3$, as is known from the literature, have relatively low mechanical characteristics: Young's modulus $E = 70.3$ GPa (a value characterizing the ability of a substance to resist longitudinal tension or compression during elastic deformation) and tensile strength $\sim 0.0218-0.0417$ N/m [9,10]. For graphene, Young's modulus $E \approx 900-1200$ GPa and tensile strength $\sim 42$ N/m [11–13]. It has been shown that the growth of $MoS_2$ layers on graphene is accompanied by an improvement in the mechanical properties of the resulting heterostructure (an increase in Young's modulus, bending modulus, tensile strength and deformation), i.e. mechanical strengthening of heterostructures is observed, provided by the graphene layer [14].

This work examines the growth of heterostructures of the topological insulator $Bi_2Se_3$ and the influence of the presence or absence of a graphene layer on the flexibility of the resulting heterostructures. As discussed in the work [6], selective growth of $Bi_2Se_3$ layers on graphene is observed, which makes it possible to obtain layers with high conductivity and charge carrier mobility. This work presents the results of a study of $Bi_2Se_3$ layers or $Bi_2Se_3$/G heterostructures (hereinafter „G" means graphene) transferred to a flexible polyethylene terephthalate (PET) substrate It has been shown that an increase in $Bi_2Se_3$ on CVD graphene leads to a significant decrease in the response of the structure (change in resistance) to tensile strains arising during bending.

## 1. Methodologies of creating samples and their research

In this work, two types of graphene layers were used:

1. Graphene was grown on copper by CVD and then transferred to a $SiO_2$/Si substrate to grow a second layer of $Bi_2Se_3$.

Parameters of the studied heterostructures: thicknesses of grown or printed graphene layers G and $Bi_2Se_3$, G1 is CVD graphene, G2 is printed graphene layer, sheet resistance of heterostructures $\rho$ and their resistance $R$ before and after transfer to a flexible substrate respectively

| Samples | Transfer method | Graphene layer thickness, nm | Thickness$Bi_2Se_3$, nm | $\rho$ (structures on $SiO_2$/Si), kΩ/sq | $R$ (PET structures), kΩ |
|---|---|---|---|---|---|
| BS/PET | Laminator | – | 20–40 | 0.9–1.5 | 10–30 |
| BS/G1/PET | Polycarbonate | ∼ 1 | 20–40 | 0.5–1.2 | 7–150 |
| BS/G2/PET | Polycarbonate | 6–8 | 20–40 | 1–3 | 5–20 |

2. Using multigraphene particles with a thickness from 0.4 to 3 nm and a size of 100–400 nm using an inkjet 2*D* printer, a layer was printed on the surface of the $SiO_2$/Si substrate; the thickness of the printed layer was ∼ 6–8 nm.

$Bi_2Se_3$ heterostructures on graphene (BS/G) were obtained by vapor-phase deposition at 500°C within the framework of the State Assignment of the IGM SB RAS 122041400031-2 [15]. The growth time was 1–1.5 h. The thickness of the grown layer was determined using anatomic-force microscopy and was 20–40 nm. With increasing distance from the source, the thickness of the $Bi_2Se_3$ layer decreased. To transfer heterostructures onto a flexible PET substrate, a polycarbonate film was used, followed by its removal in chloroform. For comparison, $Bi_2Se_3$ layers grown on mica and transferred to PET using a laminator were used.

Thus, in this work, three types of samples were used; their data and symbols are given in the table. It should be noted that graphene and the film of printed graphene had *p*-type conductivity, and the grown layers $Bi_2Se_3$ or *n*-type of conductivity, i.e. for heterostructures, a vertical $p-n$ transition was formed.

For 2*D* printing of graphene layers, a DMP-2831 Dimatix FUJIFILM inkjet printer (Fujifilm, Lebanon, PA, USA) was used. CVD graphene was purchased from company Rusgrafen, Moscow. Analysis of the surface morphology of layers and structures, as well as measurement of the thickness of grown layers, was carried out using a Solver PRO NT-MD atomic force microscope (AFM) in contact and semi-contact modes. Raman spectra when excited by radiation with a wavelength of 532 nm were obtained on Horiba Jobin Yvon LabRAM HR800 spectrometer with a LN/CCD detector. Keithley picoammeter (model 6485) was used to measure current-voltage characteristics, and two silver paste contacts were made to the films. To diagnose the grown films, the sheet resistance $\rho = RW/L$ was calculated (in Ω/sq), where $R$ is the measured resistance of the grown film, $W$ and $L$ are width and length of the tested structure, respectively. In the case of testing large-area starting films or structures, a JANDEL 4 point probe head and an HM21 Test Unit (Jandel Engineering Limited, Limslade, UK) were used and measurements were carried out at room temperature.

Deformation for testing layers and heterostructures was created by bending the structures. The formula for calculating tensile deformation in work: $\varepsilon = d/2R$, where $d$ is structure thickness, $R$ is substrate bending radius. The thickness of the flexible PET substrate was 100 $\mu$m; the thickness of the graphene and $Bi_2Se_3$ layers against the background of the substrate can be neglected.

## 2. Results and discussion

Figure 1, *a, b* shows the RS for the PET substrate and for the $Bi_2Se_3$ layer transferred to the PET substrate. In the spectra for the $Bi_2Se_3$ layer, three characteristic peaks were observed at 71, 130 and 173 $cm^{-1}$, which correspond to the out-of-plane vibrational mode ($A^1_{1g}$) of the Bi-Se pair, the plane mode ($E^2_g$) and the mode ($A^2_{1g}$) of vibrations of the rhombohedral lattice $Bi_2Se_3$ [16]. The peak in the region of 250–300 $cm^{-1}$ associated with the oxidation of $Bi_2Se_3$ is absent in the RS. A typical RS for the initial layer of printed graphene is shown in the inset of Fig. 1, *d*. RS for heterostructures BS/G1 and BS/G2 are shown in Fig. 1, *c, d*. Peaks *D*, *G* and 2*D* correspond to graphene [17,18]. The *G* line (∼ 1580 $cm^{-1}$) corresponds to the *C*–*C* vibration mode in the graphene plane, and the process of its occurrence is a typical first-order process, and the 2*D* peak is associated with second-order intervalley Raman processes. High-quality CVD graphene is characterized by a low intensity of the defect-related peak *D* and a high ratio of the intensity of the 2*D* peak to the intensity of the *G* peak. The high intensity of peak *D* compared to the intensity of peak *G* in the insert of Fig. 1, *d* for printed graphene is due to the use of relatively small graphene particles when printing the graphene layer. This dependence is due to the fact that for particles with a small lateral size, the proportion of edge atoms with dangling bonds per unit area of the material is significantly higher compared to larger in diameter particles or layers.

AFM images for $Bi_2Se_3$ films grown on top of different types of graphene layers are shown in Fig. 2. In the case of growth on CVD graphene, the film is formed more evenly than when growing on printed graphene. In the case of growth on printed graphene, $Bi_2Se_3$ first grows on each graphene particle individually and only then grows together into a single film. In the case of growth of the $Bi_2Se_3$ layer on CVD graphene (Fig. 2, *a*), selective growth is observed when the growth rate on the graphene surface is noticeably higher than the growth rate on $SiO_2$/Si. After transferring

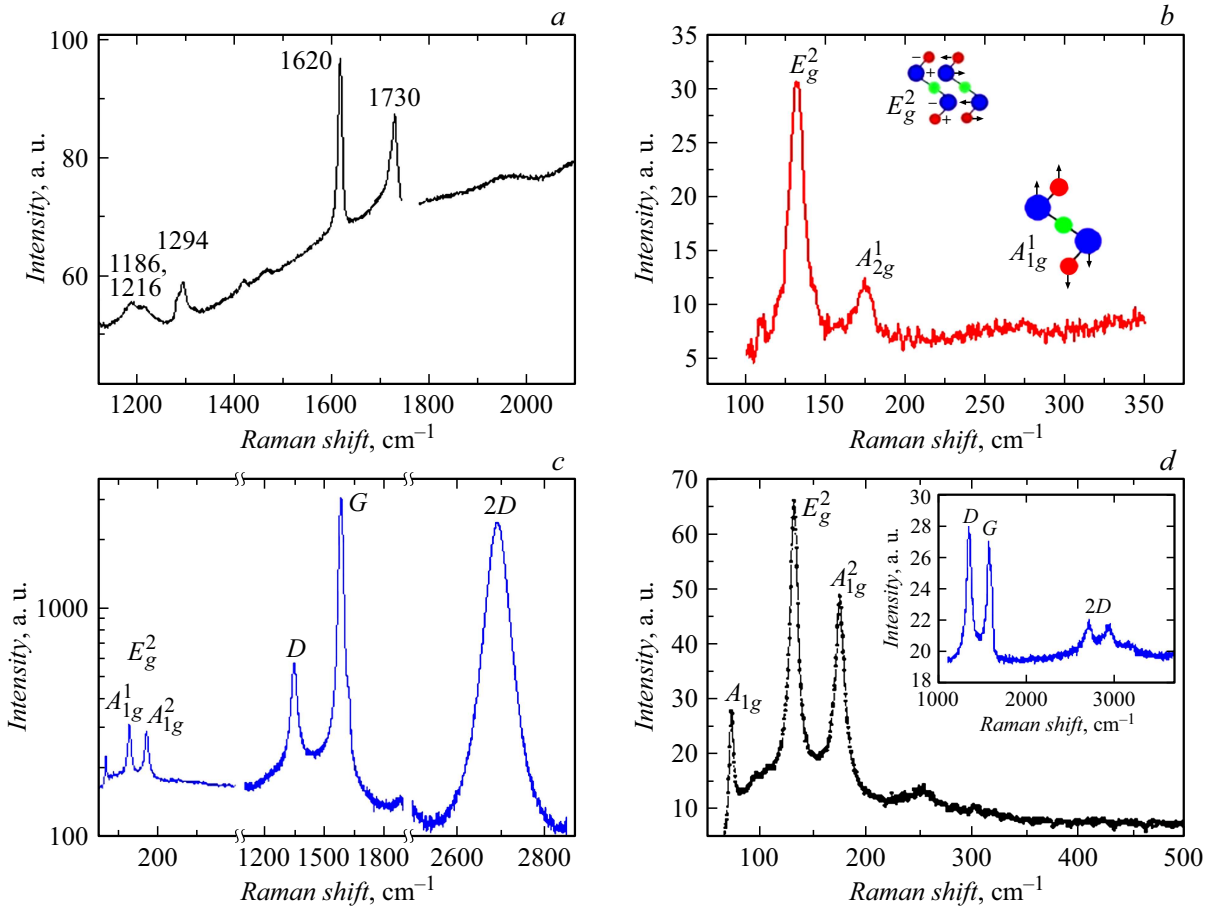


**Figure 1.** RS for a flexible PET substrate (*a*) and a film $Bi_2Se_3$ grown on mica and transferred to PET (*b*); *c* — RS for films $Bi_2Se_3$ on CVD graphene; *d* — Raman spectra for $Bi_2Se_3$ films on printed graphene The insert corresponds to the range of peaks associated with graphene.

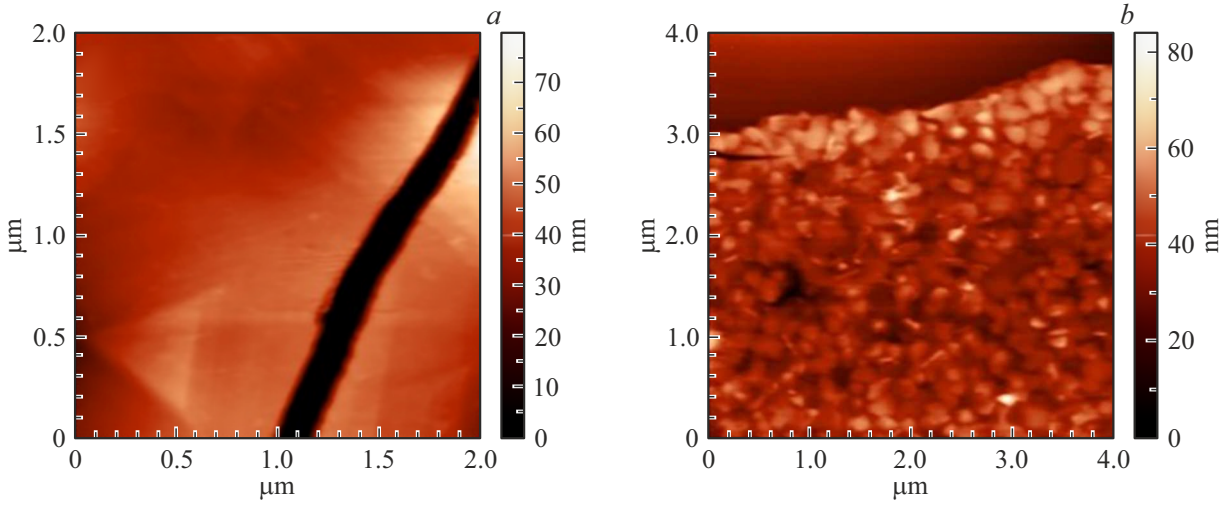


**Figure 2.** Images of the surface of $Bi_2Se_3$ layers obtained using AFM: *a* — BS/G1/PET structure (layer $Bi_2Se_3$ grown on top of CVD graphene); *b* — BS/G2/PET structure ($Bi_2Se_3$ layer grown on the surface of printed graphene). $Bi_2Se_3$ layers were grown under identical growth conditions, and after growth, the resulting structures were transferred to a flexible PET substrate.

the resulting heterostructures onto a flexible substrate, their resistance was measured depending on the tensile strains arising during bending. Figure 3–5 shows the current-voltage characteristics and resistance values for BS/PET,

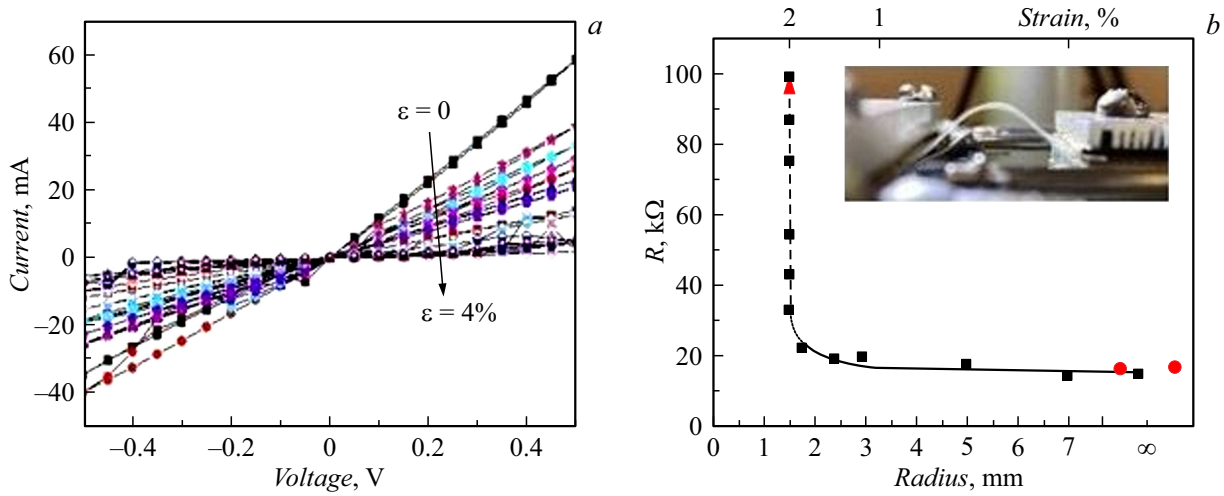


**Figure 3.** *a* — current-voltage characteristics before bending and at different deformations for the BS/PET structure (no graphene layer); *b* — dependence of resistance on bending radius (tensile deformation). Red dots correspond to the resistance of the structure after deformation is removed. The red arrow indicates an increase in resistance with repeated deformations. The insert shows a photograph of the structure being measured.

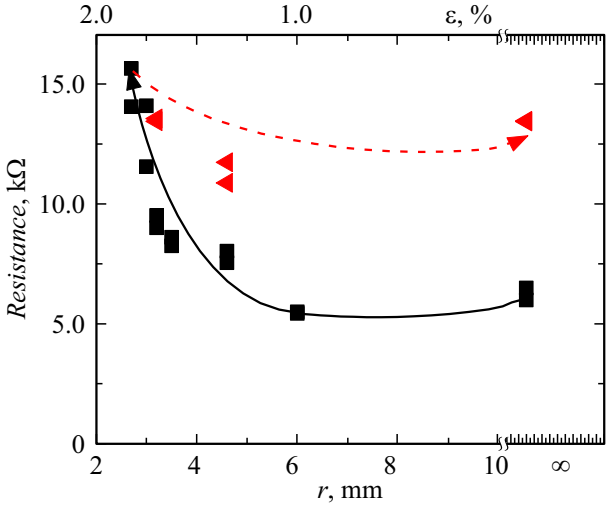


**Figure 4.** Dependence of resistance on bending radius $r$ (or tensile strain $\varepsilon$) for a BS/G2/PET structure grown on a layer of printed graphene. Square dots correspond to a decrease in the bending radius (an increase in the magnitude of tensile deformations). Triangular symbols correspond to resistance measurements as strain decreases.

BS/G1/PET and BS/G2/PET structures depending on the bending of the structures.

In Fig. 3 shows that for the BS/PET structure ($Bi_2Se_3$ layer after transfer to PET, without a graphene layer), deformations lead to a sharp decrease in the current through the structure, i.e. to an increase in sheet resistance. With an increase in tensile strain of more than 1.7%, the resistance increased from 15 to 33 k Ω, which is 120%. That is, the changes in resistance were quite significant. Repeated measurements at a bending radius of 1.5 mm (1.7% deformation) showed that further degradation of the layer occurs when it is kept in a bent state. The measurements were carried out on several samples and such a sharp increase in resistance, as shown in Fig. 3, *b*, was reproduced on all samples. Removal of deformation also led to the restoration of the original resistance. Deformations ~ 2% and more led to an irreversible increase in resistance due to ruptures of the $Bi_2Se_3$ layer.

The change in resistance of BS/G2/PET heterostructures under conditions of tensile deformation is shown in Fig. 4. As noted above, in the case of growth on printed graphene, $Bi_2Se_3$ grows on each graphene particle individually and gradually grows together into a single film. The resistance changes significantly already at tensile deformations of more than 1.5%. Moreover, no recovery of resistance is observed. This may be due to disturbances in the film structure in the thinnest and most fragile junctions of individual particles.

Fig. 5 shows data on the change in resistance in two BS/G1/PET structures grown on the surface of CVD graphene, depending on the bending radius and with gradual removal of deformation. The structures had different geometric parameters and, apparently, different defects in the graphene layer. It can be seen that bending up to a radius of 1.5 mm (corresponding to a deformation of 3.2%) leads to a relatively weak increase in resistance for both samples; the increase is ~ 20–30%. After the deformation was removed, the resistance was completely restored.

Comparing the three types of structures studied with a thickness of$Bi_2Se_3$ 20–40 nm, it must be stated that the use of a CVD graphene sublayer significantly reduces the change in resistance (up to 20–25%) with tension up to 3.3% (structure BS/G1/PET). The structure without graphene (BS/PET) withstood only 1.7% of tensile deformations. The structure on printed graphene (BS/G2/PET), due to the inhomogeneity of the $Bi_2Se_3$ layer in thickness in the areas of particle connection growing on individual

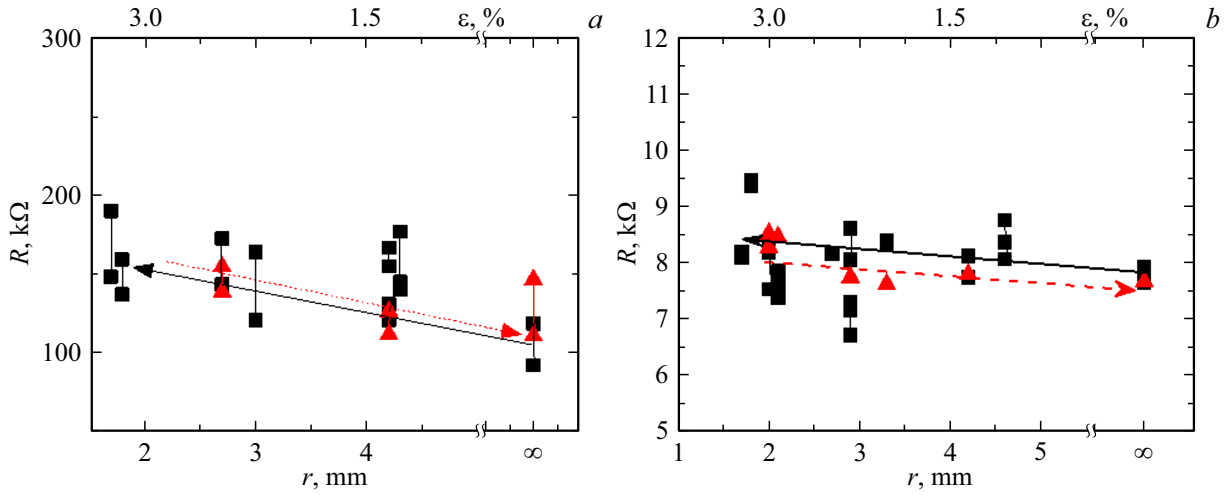


**Figure 5.** Dependence of resistance on bending radius $r$ (tensile deformation $\varepsilon$) for two BS/G1/PET structures. Square dots correspond to a decrease in the bending radius (an increase in the magnitude of tensile deformations). Triangular symbols and a dotted arrow indicate the reversal of resistance measurements as strain decreases.

graphene particles, demonstrated an irreversible increase in tension of 1.5%.

The more stable properties of $Bi_2Se_3$ layers grown on CVD graphene are not associated with the simple participation of graphene in conductivity, since $Bi_2Se_3$ and graphene have different types of conductivity ($Bi_2Se_3$ — *n*-type of conductivity and graphene — *p* conductivity type). The reason is associated with the improved properties of the $Bi_2Se_3$ layer when grown directly on graphene, and, in particular, with the higher mobility of charge carriers in the $Bi_2Se_3$ layers and the better structure of the layers [19]. A slight and reversible increase in resistance in BS/G1/PET heterostructures is associated with a known decrease in conductivity and carrier mobility in 2*D*-materials under tensile deformation [20].

Thus, a significant improvement in the mechanical properties of thin layers of the topological insulator $Bi_2Se_3$ is demonstrated when it grows on CVD graphene, which suggests the possibility of using these layers for flexible electronics.

## Conclusions

The use of $Bi_2Se_3$ heterostructures on CVD graphene leads not only to a better structure and high conductivity of the $Bi_2Se_3$ layer, but also to an improvement in its mechanical properties. Films $Bi_2Se_3$ with a thickness of 20–40 nm based on CVD graphene slightly changed their resistance under tensile deformations created during bending of the structures. It was found that the resistance increases by 20–25% when stretched to 3%. Similar films $Bi_2Se_3$ without graphene could withstand only 2% stretching. In structures on printed graphene, due to the inhomogeneity of the $Bi_2Se_3$ layer in thickness in the areas of connection of particles growing on individual graphene particles, partial destruction of these connections with an irreversible increase in resistance is apparently observed. Thus, $Bi_2Se_3$ heterostructures on CVD graphene are promising for use in flexible electronics.

### Acknowledgments

Raman spectra were recorded using the equipment of the Collective Use Center „VTAN“ of Novosibirsk State University.

### Funding

The work was supported by the Ministry of Science and Higher Education of the Russian Federation (075-15-2020-797, 13.1902.21.0024).

### Conflict of interest

The authors declare that they have no conflict of interest.

## References

[1] X. Li, L. Tao, Z. Chen, H. Fang, X. Li, X. Wang, J.-B. Xu, H. Zhu. Appl. Phys. Rev., **4**, 021306 (2017). DOI: 10.1063/1.4983646

[2] T.D. Thanh, N.D. Chuong, H.V. Hien, T. Kshetri, L.H. Tuan, N.H. Kim, J.H. Lee. Prog. Mat. Sci., **96**, 51 (2018). DOI: 10.1016/j.pmatsci.2018.03.007

[3] J.A. Miwa, M. Dendzik, S.S. Grönborg, M. Bianchi, J.V. Lauritsen, P. Hofmann, S. Ulstrup. ACS Nano, **9** (6), 6502 (2015). DOI: 10.1021/acsnano.5b02345

[4] J.M. Woods, Y. Jung, Y.J. Xie, W. Liu, Y. Liu, H. Wang, J.J. Cha. ACS Nano, **10** (2), 2004 (2016). DOI: 10.1021/acsnano.5b06126

[5] C. Zhang, C. Li, J. Yu, S. Jiang, S. Xu, C. Yang, Y.J. Liu, X. Gao, A. Liu, B. Man. Sens. Actuat. B Chem., **258**, 163 (2018). DOI: 10.1016/j.snb.2017.11.080

[6] I.V. Antonova, K.A. Kokh, N.A. Nebogatikova, E.A. Suprun, V.A. Golyshov, O.E. Tereshenko. Crystal Growth and Design, **22** (9), 5335 (2022). DOI: 10.1021/acs.cgd.2c00431
[7] X. Gao, M. Zhou, Y. Cheng, G. Ji. Philosophical Magazine, **96** (2), 208 (2016). DOI: 10.1080/14786435.2015.1128126
[8] A. Politano, G. Chiarello. Nano Research, **8**, 1847 (2015) DOI: 10.1007/s12274-014-0691-9
[9] K. Song, D. Soriano, A.W. Cummings, R. Robles, P. Ordejón, S. Roche. Nano Lett., **18** (3), 2033 (2018). DOI: 10.1021/acs.nanolett.7b05482
[10] C. Lee, X. Wei, J.W. Kysar, J. Hone. Science, **321** (5887), 385 (2008). DOI: 10.1126/science.1157996.
[11] H. Qiao, J. Yuan, Z. Xu, C. Chen, S. Lin, Y. Wang, J. Song, Y. Liu, Q. Khan, H.Y. Hoh, C.-X. Pan, S. Li, Q. Bao. ACS Nano, **9** (2), 1886 (2015). DOI: 10.1021/nn506920z
[12] G. Cao. Polymers, **6** (9), 2404 (2014). DOI: 10.3390/polym6092404
[13] H. Yan, C. Vajner, M. Kuhlman, L. Guo, L. Li, P.T. Araujo, H.-T. Wang. Appl. Phys. Lett., **109** (3), 032103 (2016). DOI: 10.1063/1.4958986
[14] R.M. Elder, M.R. Neupane, T.L. Chantawansri. Appl. Phys. Lett., **107** (7), 073101 (2015). DOI: 10.1063/1.4928752
[15] K.A. Kokh, N.A. Nebogatikova, I.V. Antonova, D.A. Kustov, V.A. Golyashov, E.S. Goldyreva, N.P. Stepina, V.V. Kirienko, O.E. Tereshchenko. Materials Research Bulletin, **129**, 110906 (2020). DOI: 10.1016/j.materresbull.2020.110906
[16] J. Zhang, Z. Peng, A. Soni, Y. Zhao, Y. Xiong, B. Peng, J. Wang, M.S. Dresselhaus, Q. Xiong. Nano Lett., **11** (6), 2407 (2011). DOI: 10.1021/nl200773n
[17] S. Ryu, J. Maultzsch, M.Y. Han, P. Kim, L.E. Brus. ACS Nano, **5** (5), 4123 (2011). DOI: 10.1021/nn200799y
[18] A.C. Ferrari, J. Robertson. Phys. Rev B, **61** (20), 14095 (2000). DOI: 10.1103/PhysRevB.61.14095
[19] I.V. Antonova, N.A. Nebogatikova, N.P. Stepina, V.A. Volodin, V.V. Kirienko, M.G. Rybin, E.D. Obrazstova, V.A. Golyashov, K.A. Kokh, O.E. Tereshchenko. J. Mater. Sci., **56**, 9330 (2021). DOI: 10.1007/s10853-021-05836-y
[20] X. He, L. Gao, N. Tang, J. Duan, F. Xu, X. Wang, X. Yang, W. Ge, B. Shen. Appl. Phys. Lett., **105** (8), 083108 (2014). DOI: 10.1063/1.4894082

*Translated by V.Prokhorov*